

Anticrossing and coupling of light-hole and heavy-hole states in (001) GaAs/Al_xGa_{1-x}As heterostructures

Rita Magri

Istituto Nazionale per la Fisica della Materia e Dipartimento di Fisica, Università di Modena e Reggio Emilia, Modena, Italy

Alex Zunger

National Renewable Energy Laboratory, Golden, Colorado 80401

(Received 15 May 2000)

Heterostructures sharing a common atom such as AlAs/GaAs/AlAs have a D_{2d} point-group symmetry which allows the bulk-forbidden coupling between odd-parity light-hole states (e.g., lh1) and even-parity heavy-hole states (e.g., hh2). Continuum models, such as the commonly implemented (“standard model”) $\mathbf{k}\cdot\mathbf{p}$ theory miss the correct D_{2d} symmetry and thus produce zero coupling at the zone center. We have used the atomistic empirical pseudopotential theory to study the lh1-hh2 coupling in (001) superlattices and quantum wells of GaAs/Al_xGa_{1-x}As. By varying the Al concentration x of the barrier we scan a range of valence-band barrier heights $\Delta E_v(x)$. We find the following: (i) The lh1 and hh2 states anticross at rather large quantum wells width or superlattice periods $60 < n_c < 70$ monolayers. (ii) The coupling matrix elements $V_{lh1,hh2}^{k_{\parallel}=0}$ are small (0.02–0.07 meV) and reach a maximum value at a valence-band barrier height $\Delta E_v \approx 100$ meV, which corresponds to an Al composition $x_{Al}=0.2$ in the barrier. (iii) The coupling matrix elements obtained from our atomistic theory are at least an order of magnitude smaller than those calculated by the phenomenological model of Ivchenko *et al.* [Phys. Rev. B **54**, 5852 (1996)]. (iv) The dependence of $V_{lh1,hh2}$ on the barrier height $\Delta E_v(x)$ is more complicated than that suggested by the recent model of Cortez *et al.*, [J. Vac. Sci. Technol. B **18**, 2232 (2000)], in which $V_{lh1,hh2}$ is proportional to the product of $\Delta E_v(x)$ times the amplitudes of the lh1 and hh2 envelopes at the interfaces. Thus, atomistic information is needed to establish the actual scaling.

I. INTRODUCTION

A. The three classes of light-hole–heavy-hole coupling in semiconductor heterostructures

Quantum states that belong to the same symmetry representation mix and anticross in the presence of a perturbation. The anticrossing effect on electronic energy levels of solids is often very significant, and includes the occurrence of “band-gap bowing” in random alloys,¹ band-gap narrowing in ordered vs random alloys,² saturation of impurity levels with pressure,³ and “ p - d repulsion” in II-VI (Ref. 4) or I-III-VI₂ (Ref. 5) compounds affecting band offsets and spin-orbit splitting. Here we focus on the consequences of level anticrossing in (001) semiconductor superlattices and quantum wells made of zinc-blende constituents. In the zinc-blende structure the valence-band maximum (VBM) is a four-degenerate Γ_{8v} state (including spin-orbit coupling), while the conduction-band minimum is the twofold degenerate Γ_{6c} state. The Γ_{8v} contains light-hole (lh) and heavy-hole (hh) components. The optical transitions $lh \rightarrow e$ and $hh \rightarrow e$ to the first electron level e are allowed in the bulk and have isotropic polarization. When one forms a (001)-oriented quantum well from zinc-blende components, there are three different effects on the electronic states: (i) The zinc-blende bands between $\Gamma(000)$ and $X(001)$ fold into $k_{\parallel}=0$ of the quantum well thus adding new states, (ii) the reduced superlattice symmetry from T_d can split Γ_{8v} , and (iii) the strain arising from size mismatch can also split Γ_{8v} . This last effect is absent in lattice-matched components such as GaAs and AlAs. In GaAs/AlAs heterostructures effects (i) and (ii)

give rise to a series of hole levels $hh1 < lh1 < hh2 \dots$ and electron states $e1 < e2 < \dots$ at $k_{\parallel}=0$.

Coupling exists between states of the same symmetry. This is decided as follows. A *single* zinc-blende (001) interface has C_{2v} symmetry.⁶ If one forms a structurally perfect quantum well from two semiconductors sharing one chemical specie in common (i.e., a “pseudobinary system” such as GaAs-AlAs or GaAs-InAs), the overall symmetry of *both interfaces* is D_{2d} . If the interfaces are not structurally perfect or if the two semiconductors have no atom in common (i.e., quaternary systems such as InP-GaAs or InAs-GaSb) (Ref. 7) then the overall symmetry of the two interfaces is lowered back to C_{2v} . The lowering of the symmetry of the superlattice from T_d to either C_{2v} or D_{2d} can give rise to an in-plane [i.e., (110) vs (−110)] polarization anisotropy of interband transitions dipole α between states i and j , which is measured by the polarization ratio λ_{ij} ,

$$\lambda_{ij} = \frac{\alpha_{110}^{ij} - \alpha_{\bar{1}\bar{1}0}^{ij}}{\alpha_{110}^{ij} + \alpha_{\bar{1}\bar{1}0}^{ij}}. \quad (1)$$

In the absence of level coupling, the dipole-allowed transitions in the superlattice are $lh1-e1$ [polarized along $z=(001)$ and in the xy plane]; $hh1-e1$ (polarized *only* in the xy plane), and $hh2-e2$ (polarized *only* in the xy plane). Thus, only transitions between electron and hole states having the same parity (odd or even) with respect to the z axis are dipole allowed in superlattices. However, perturbative mixing of levels can transform parity-forbidden transitions to allowed transitions, and produce a nonvanishing polarization anisot-

TABLE I. Light-hole and heavy-hole couplings at $\mathbf{k}_{\parallel}=0$ for the first three subbands in common and no-common atom zinc-blende heterostructures grown along the [001] axis. $V_{lh1,hh1}$ is responsible for the in-plane polarization anisotropy (PA) λ [Eq. (1)] of the interband transitions to electron states, while the $V_{lh1,hh2}$ coupling is responsible for the appearance of lh1- $e2$ and hh2- $e1$ forbidden transitions. Standard $\mathbf{k}\cdot\mathbf{p}$ implementations produce $V_{lh,hh}=0$ at $\mathbf{k}_{\parallel}=0$ in all of the cases below.

System	$V_{lh1,hh1}$	$V_{lh1,hh2}$	PA
A single (001) interface, e.g., (AlAs/GaAs): C_{2v}	nonzero	nonzero	$\lambda \neq 0$
Two different (001) interfaces with no-common atom C_{2v} , e.g., (InAs/GaSb/InAs): C_{2v}	nonzero	nonzero	$\lambda \neq 0$
Two equal (001) interfaces with a common atom, e.g., (AlAs/GaAs/AlAs): D_{2d}	zero	nonzero	$\lambda = 0$

ropy $\lambda \neq 0$. The nature of the level mixing depends on symmetry. There are three cases: (i) A single zinc-blende interface; the symmetry is C_{2v} . (ii) Two different interfaces in systems that do not share a common atom; the symmetry is C_{2v} . (iii) Two interfaces in systems that share a common atom; the symmetry is D_{2d} . Two equal interfaces in no-common atom systems in (001) superlattices with a noninteger period also have D_{2d} symmetry. We next describe briefly these cases summarized in Table I. In this paper we concentrate mainly on case (iii).

(i) *A single zinc-blende interface: C_{2v} .* A single interface can be grown intentionally. Alternatively, if two interfaces of a quantum well made of common-atom pair have some growth defect (e.g., due to segregation), then the combined C_{2v} symmetries of the individual interfaces do not add up to a D_{2d} symmetry, but instead the C_{2v} symmetry of a single interface survives. Even if the two interfaces are defect-free, one can break the symmetry relation of the two interfaces in a quantum well by applying an electric field in the growth direction. In all of these cases the lower C_{2v} symmetry breaks the degeneracy at the VBM and leads to a coupling between the components of Γ_{8v} at $\mathbf{k}_{\parallel}=0$. In a quantum well or superlattice where the states are described as the product of a Bloch state of the zinc-blende parent compound at $\mathbf{k}_{\parallel}=0$ times an envelope function, this mixing is translated into the coupling of the states which have the same symmetry representation under C_{2v} (and thus can mix and anticross). These are lhn and hhm for any quantum index n and m . Thus, lh1 can mix with hh1 in C_{2v} . As a consequence of these mixings, parity-forbidden transitions and an in-plane polarization anisotropy of the optical properties can be observed. This was seen in photoluminescence and reflectance difference spectroscopy experiments on GaAs/AlAs after the application of an electric field along the growth direction (the quantum confined Pockels effect^{8,9}) or in the case of AlAs/GaAs/Al_xGa_{1-x}As asymmetric quantum wells.¹⁰ The effect of the electric field on common atom GaAs/AlAs quantum wells is twofold: (a) by lowering the symmetry to C_{2v} it allows the mixing of lh and hh states with the same parity (i.e., lh1 and hh1), (b) the field breaks the parity symmetry of all the hole and electron states and allows the lh1 and hh2 coupling to be observed experimentally through a strong polarization anisotropy of the emission of the nominally forbidden excitons (i.e., hh2- $e1$ and hh1- $e2$).⁸

Among the experimental studies addressing the symmetry properties of the single (001) interface is the work of Gour-

don and Lavallard¹¹ who studied the features of a previously reported small splitting (a few μeV) of heavy excitons in type-II GaAs/AlAs superlattices. The authors could account for the observed splitting by assuming that the superlattice had a C_{2v} symmetry, not the nominal D_{2d} symmetry. The physical origin of the C_{2v} symmetry was attributed to different degrees of interfacial roughness which causes an asymmetry between the [110] and $[-110]$ directions at the (001) interfaces, together with the biaxial compression of the AlAs layers. Another paper addressing the additional exchange splitting in type-II GaAs/AlAs superlattices is the theoretical work of Pikus and Pikus,¹² who have proposed two models to explain the origin of the symmetry reduction to C_{2v} and hole mixing: a local deformation in the GaAs well, or the fact that localized exciton in type-II short-period structures sees only one interface. Edwards and Inkson,¹³ using an empirical pseudopotential formalism, studied the hole scattering at a (001) GaAs/AlAs single interface (C_{2v}), and found a strong bulk light-hole-heavy-hole mixing at $\mathbf{k}_{\parallel}=0$.

(ii) *Two interfaces that do not share a common atom: C_{2v}* This case corresponds to no-common atom InAs/GaSb or (GaIn)As/InP systems with two different interfaces discussed in Refs. 7, 14–16. In this case a giant in-plane optical anisotropy has been found in absorption measurements⁷ even without application of electric fields. The asymmetric potential along the growth direction is supplied by the inequivalence of the (001) interfaces which lowers the overall symmetry from D_{2d} to the C_{2v} point group. The anisotropy is largest at the onset of absorption in type-I superlattices (GaIn)As/InP implying⁷ a strong coupling between hh1 and lh1 at the top of the valence band at $\mathbf{k}_{\parallel}=0$. Recently the polarization anisotropy in no-common atom systems has been investigated by atomistic *ab initio*¹⁴ and semiempirical^{15,16} pseudopotential methods. An atomistic semiempirical pseudopotential scheme¹⁵ has indeed found a polarization anisotropy of the $h1-e1$ transition at $\mathbf{k}_{\parallel}=0$ in type-II semiconducting InAs/GaSb superlattices. Note that this anisotropy cannot be predicted by “standard” $\mathbf{k}\cdot\mathbf{p}$ theories which produce zero heavy and light hole coupling, $V_{lh,hh}=0$, at $\mathbf{k}_{\parallel}=0$. A consequence of hh1 and lh1 coupling in the real InAs/GaSb systems is the occurrence of nonzero coupling $V_{e1,hh1} \neq 0$ between the electron state $e1$ and the heavy-hole state hh1 at $\mathbf{k}_{\parallel}=0$ found for superlattices $(\text{InAs})_n/(\text{GaSb})_n$ with $n \approx 28$.¹⁵ The eight band $\mathbf{k}\cdot\mathbf{p}$ theory, which yields $V_{e1,hh1}^{\mathbf{k}_{\parallel}=0} = 0$, has predicted instead a simple crossing. On the other

hand, the $\mathbf{k}\cdot\mathbf{p}$ theory is capable of describing couplings at $\mathbf{k}_{\parallel}\neq 0$ and thus has produced results similar to those of atomistic theories for the hybridization gaps at $\mathbf{k}_{\parallel}\neq 0$ in nominally semimetallic $(\text{InAs})_n/(\text{GaSb})_n$ superlattices with $n > 28$.¹⁶

(iii) *Two interfaces of a common-atom heterostructure: D_{2d} .* The states that have the same symmetry representation (and hence can mix and anticross) under D_{2d} are hh even with lh odd (such as hh2 and lh1) or hh odd with lh even (such as hh1-lh2). The lh1-hh1 coupling is forbidden. In the D_{2d} case there is no in-plane polarization anisotropy [$\lambda=0$ in Eq. (1) for all interband transitions], since the two interfaces are equal, and the [110] and $[-110]$ crystal directions are equivalent. However, new nominally forbidden transitions $\text{hh2}\rightarrow e1$ and $\text{lh1}\rightarrow e2$ can be observed in D_{2d} . This is because in the presence of the lh1 and hh2 coupling, “hh2” (“lh1”) is no longer pure hh2 (lh1) character but has some weight on the lh1 (hh2) hole state. Some experimental evidence of lh1-hh2 coupling in common atom superlattices was reported in the literature. Miller *et al.*¹⁷ observed strong parity-forbidden excitons $\text{hh2-}e1$ and $\text{lh1-}e2$ in photoluminescence excitation spectra, whose intensity could not be fully explained by a theory neglecting the hh2 and lh1 mixing at $\mathbf{k}_{\parallel}=\mathbf{0}$. Two forbidden ground state $\text{hh2-}e1$ and $\text{hh3-}e1$ excitons were observed in photoreflectance and photoluminescence excitation experiments by Theis *et al.*¹⁸ The theoretical treatment used in that paper to assign the experimental features in the spectrum did not take valence subband mixing effects into account and was thus unable to describe the two forbidden features. Chang and Schulman¹⁹ studied the electronic states of $(\text{GaAs})_n/(\text{AlAs})_n$ superlattices using a tight-binding approach and showed that the second and the third superlattice valence bands exchange their character at periods $20 < n < 50$. For small well widths lh1 was more bound than hh2, since it corresponds to the lowest-energy eigenvalue, while for longer well widths, hh2 became more bound, since it has a much higher effective mass. Thus, at some well width L_c or superlattice period n_c , the lh1 and hh2 states should anticross. These pioneering atomistic calculations predicted the appearance of the forbidden hh2 to $e1$ transition, because of the lh1 and hh2 coupling.

B. Atomistic vs continuum $\mathbf{k}\cdot\mathbf{p}$ descriptions of lh-hh coupling in heterostructures

Table I summarizes the cases where coupling between light-hole and heavy-hole states is symmetry allowed. It is important to realize that the “standard model” of heterostructure electronic structure, the conventional²⁰ $\mathbf{k}\cdot\mathbf{p}$ approach, produces zero coupling at $\mathbf{k}_{\parallel}=\mathbf{0}$ for all cases noted in the table. In the $\mathbf{k}\cdot\mathbf{p}$ method the nanostructure wave functions are expanded in a set $\{\phi_{n,\Gamma}\}$ of Γ -like Bloch states of a zinc-blende crystal. If one were to use a complete set $\{\phi_{n,\Gamma}\}$, the results would be exact. In practice, one makes the envelope-function approximation and retains only $n=\Gamma_{8v}+\Gamma_{7v}$ (six states, including spin) plus $n=\Gamma_{6c}$ (two states, including spin). This minimal basis set, including only the VBM and conduction-band minimum (CBM) is unable to resolve any atomistic detail in the wave function of the nanostructure. Thus, the standard $\mathbf{k}\cdot\mathbf{p}$ method does not “see” the correct point-group symmetries C_{2v} and D_{2d} of Table I, con-

fusing them instead with the zinc-blende symmetry T_d of the *basis* functions. As a result, all mixing potentials $V_{\text{lh, hh}}^{\mathbf{k}_{\parallel}}=0$ and the polarization anisotropy $\lambda=0$ in all cases. In contrast, any atomistic approach [tight-binding,^{19,21} linear combination of atomic orbitals (LCAO), pseudopotentials] which constructs the total potential of the nanostructure as a superposition of the potentials of all atomic species at their corresponding locations, must, by definition, recognize the correct point-group symmetry, and produce nonzero coupling (unless the matrix elements are approximated²²).

While atomistic approaches^{14–16,19,21} to the electronic structure of nanostructures *force upon us* the correct symmetry of the system, thus producing state mixing in the lower symmetry space group, the “standard” model of the $\mathbf{k}\cdot\mathbf{p}$ approach *can only accommodate* state mixing if it is added *ex post facto* “by hand.”

The state mixing can be ultimately related to the existence (D_{2d}) and to the symmetry (C_{2v}) of the (001) interfaces. The main problem of the $\mathbf{k}\cdot\mathbf{p}$ approaches derives usually by a simplified description of the superlattice potential. In the most common implementations the interfaces between different materials are treated as step functions (the step being determined by the valence-band offset), and any other mixing between the bulk states which are not already inserted in the standard n -band $\mathbf{k}\cdot\mathbf{p}$ scheme have to be introduced through appropriate boundary conditions. These further couplings which are aimed to mimic the behavior of the real interfaces are termed *interface band mixings* and have recently attracted much attention.^{6,23–26} Different approaches have been used to address this problem. Most of them imply a generalization of the boundary conditions at the interfaces. This can be done either by using an “exact” $\mathbf{k}\cdot\mathbf{p}$ (Refs. 23 and 24) (which unfortunately is not still practical to implement), or by using a “model Hamiltonian” approach to the problem (Krebs and Voisin,⁷ Ivchenko *et al.*⁶) in which one adds terms to $\mathbf{k}\cdot\mathbf{p}$ that produce “by construction” the interface-mandated band couplings, but unlike atomistic approaches, the *values* of the coupling parameters are not given by the model Hamiltonian so they must be fitted externally. Smith and Mailhiot²⁵ and Burt²³ observed that a limiting assumption of the envelope-function approximation is to use the same Bloch functions for the different zinc-blende constituents. Burt²³ suggested reformulating the envelope-function approximation in order to take into account the variation of the Bloch functions at the interface: the condition of continuity of the envelope at the interface should be substituted by a condition of continuity of the entire wave function. Foreman²⁴ exploited the local symmetry of the periodic Bloch functions in zinc-blende materials and showed that the valence X and Y symmetry states are always coupled at an interface even for $\mathbf{k}_{\parallel}=\mathbf{0}$. The mixing between lh1 and hh2 in GaAs/AlAs is obtained in the generalized boundary conditions (GBC) method of Ivchenko⁶ by including appropriate off-diagonal terms into the boundary conditions for the envelopes. The coupling matrix element depends on a dimensionless heavy-hole–light-hole mixing coefficient t_{lh} whose value is obtained fitting atomistic calculations or experimental data. Estimated values of this parameter range between 0.3 and 0.9. In the Krebs and Voisin⁷ model a new term is added to the envelope-function Hamiltonian. It is a δ potential localized at the interfaces which carries the appro-

appropriate C_{2v} symmetry of the single (001) interface. This approach is substantially similar to Ivchenko's. The only difference is that the lh-hh coupling parameter is expressed in terms of the valence-band offset.²⁷

C. The purpose of the present paper and its main results

The purpose of this paper is to provide a microscopic atomistic theory for lh1-hh2 coupling in D_{2d} -type GaAs/(AlGa)As heterostructures. Using the empirical pseudopotential method we determine the period n_c where the $(\text{GaAs})_n/(\text{AlAs})_n$ superlattices and the $(\text{GaAs})_n/(\text{Al}_{1-x}\text{Ga}_x\text{As})_\infty$ quantum wells exhibit lh1-hh2 anticrossing at different values x of the barrier. By varying the composition of the barrier material we alter the magnitude of the well-to-barrier valence-band offset $\Delta E_v(x)$. Calculation of the coupling matrix element vs barrier composition then establishes $V_{lh1,hh2}^{k_{\parallel}=0}$ for different barrier heights $\Delta E_v(x)$. We find that: (i) the lh1 and hh2 states anticross at rather large quantum well widths or superlattice periods $60 < n_c < 70$ monolayers. (ii) The coupling matrix element $V_{lh1,hh2}^{k_{\parallel}=0}$ is small, being between 0.02 meV and 0.07 meV. (iii) The coupling matrix element obtained from our atomistic theory is at least an order of magnitude smaller than that inferred from the phenomenological model Hamiltonian approach of Ivchenko (using a coupling parameter $t_{lh}=0.5$).⁶ (iv) The coupling matrix element is small at low Al composition (shallow barrier), increases with barrier composition, reaching a maximum at a barrier height $\Delta E_v \approx 100$ meV (Al composition $x_{Al}=0.2$), and then decays to zero as the barrier increases. The reason for this behavior is that as ΔE_v is large (pure AlAs/GaAs interface) the wave functions are localized *inside* the well, so their amplitude at the interfaces approaches zero. Thus, the interface potential which is at the origin of the lh1-hh2 coupling has a null effect. The opposite limit, $\Delta E_v \rightarrow 0$ (interface between GaAs and Ga-rich AlGaAs) corresponds to $x_{Al} \rightarrow 0$. In this case the material at both sides of the interface is the *same*, so the T_d symmetry is restored, and $V_{lh1,hh2} \rightarrow 0$. (v) The dependence of $V_{lh1,hh2}$ on the barrier height $\Delta E_v(x)$ is more complicated than that suggested by the recent model of Cortez *et al.*,²⁷ where $V_{lh1,hh2}$ is written in terms of the product of the band offset times the amplitudes of the lh1 and hh2 envelopes at the interfaces. Thus, atomistic information is needed to establish the actual scaling. (vi) The anticrossing transition between lh1 and hh2 takes place over a very few superlattice periods (four, five) in contrast with the results of the tight-binding calculation of Chang and Schulman,¹⁹ that predict a broader transition range.

II. METHOD OF CALCULATION

We have calculated the electron and hole energies by solving the pseudopotential single-particle Schrödinger equation:

$$\left[-\frac{\nabla^2}{2} + \sum_{n\alpha} v_\alpha(r-R_{n\alpha}) \right] \psi_i(r) = \epsilon_i \psi_i(r), \quad (2)$$

where $R_{n\alpha}$ denotes the position of the n th ion of type α . For the screened atomic pseudopotentials v_α we use those devel-

oped by Mader and Zunger²⁸ for $\alpha = \text{Ga}, \text{Al}, \text{and As}$, given in Table V of Ref. 28. The same screened pseudopotentials have been used also in Ref. 29. The As potential depends on the number of Ga and Al nearest neighbors,

$$v_{As}(\text{Ga}_{4-n}\text{Al}_n\text{As}) = \frac{4-n}{4} v_{As}(\text{GaAs}) + \frac{n}{4} v_{As}(\text{AlAs}). \quad (3)$$

Equation (3) takes into account approximately the charge transfer on the As atoms which depends on the number of Ga and Al nearest neighbors. It distinguishes interfacial As (having two Al and two Ga neighbors) from bulk As (having either four Al or four Ga neighbors). We use the same $n=2$ pseudopotential for As at the two interfaces, preserving in this way the full D_{2d} symmetry of the common atom system. To test our pseudopotential we have compared our results for the extreme case of short-period $(\text{GaAs})_1/(\text{AlAs})_1$ and $(\text{GaAs})_2/(\text{AlAs})_2$ (001) superlattices with the existing *ab initio* quasiparticle calculations and experimental results.³⁰⁻³² In the case of the $(\text{GaAs})_1/(\text{AlAs})_1$ superlattice we obtain 2.02, 2.08, 2.11, and 1.95 eV for the minimum band gaps at the folded Γ , X_z , X_{xy} , and L high-symmetry zinc-blende k points, respectively, to be compared with the experimental values^{30,31} of 2.20, 2.09, 2.07 eV and, the last value with 1.85 eV available only from a quasiparticle calculation³²). In the case of the $(\text{GaAs})_2/(\text{AlAs})_2$ superlattice we obtain for the Γ , X_z , X_{xy} , and L band gaps, respectively, 2.17, 2.06, 2.08, and 2.34 eV to be compared with 2.19, 2.08, 2.07 eV (experimental values), while the last value can only be compared with the quasiparticle calculation, 2.34 eV.

The only difference between the present method of calculation and the calculations of Refs. 28 and 29 is the treatment of the spin-orbit coupling. Here the spin-orbit nonlocal potential is calculated using the "small box implementation" described in Ref. 33 while in Refs. 28 and 29 a computationally slower separable nonlocal pseudopotential approach was used. Here we expand the $\psi_i(r)$ in a set of plane waves with the same energy cutoff used to construct $v_\alpha(q)$. We solve Eq. (2) near the band gap using the folded spectrum method.³⁴ The results for the energies at the critical points and the effective masses of the binary GaAs and AlAs compounds are given in Table II.

We have neglected the atomic relaxations due to the small lattice mismatch between GaAs and AlAs, about 0.1%. Thus, all the calculations are performed using the same lattice constant $a=10.6826$ a.u. and atomic positions at the ideal zinc-blende sites. With the pseudopotential parameters given in Table V of Ref. 28, we obtain a valence-band offset $\Delta E_v=0.49$ eV between pure GaAs and AlAs.

Our atomistic approach does not suffer of the limitations of the standard envelope-function approximation in that (a) all band couplings are automatically included in the theoretical description and the bands in the binaries are correctly predicted over the entire Brillouin zone; (b) the heterostructure band dispersion is computed with the same accuracy as for the zinc-blende compounds, since no *ad hoc* assumptions are made on the shape of the potential; (c) the correct point-group symmetry is recognized automatically by the Hamil-

TABLE II. Critical point energies of bulk GaAs and AlAs as obtained in the present relativistic empirical pseudopotential method (EPM) and effective masses (in units of the electron mass m_0). The zero of energy is at Γ_{8v} , the top of the valence band.

	GaAs	AlAs
Γ_{6v}	-12.22	-11.80
Δ_0	0.36	0.30
Γ_{6c}	1.52	3.06
Γ_{7c}	3.81	4.36
X_{7v}	-2.37	-2.25
$\Delta_2(X)$	0.17	0.14
X_{6c}	1.93	2.28
X_{7c}	2.33	2.85
$L_{4,5v}$	-0.99	-0.91
Δ_1	0.21	0.17
L_{6c}	1.80	2.82
m_n	0.083	0.154
m_{hh}	0.400	0.459
m_{lh}	0.108	0.200
m_{so}	0.208	0.309

tonian; (d) one needs to fit only the bulk band structure without additional (e.g., interfacial) parameters⁶.

Finally, using the eigenstates obtained solving Eq. (2) we have calculated the interband dipole transitions-matrix elements squared $I_{i,j}(\hat{\epsilon}) = |\langle \psi_i | \hat{\epsilon} \cdot \hat{p} | \psi_j \rangle|^2$, where $\hat{\epsilon}$ is the photon polarization vector, ψ_i are the hh1, lh1, and hh2 hole states, while ψ_j are the $e1$ and $e2$ electron states at $\mathbf{k}_{\parallel}=0$. The study of the polarization-dependent oscillator strengths of the interband transitions provide further information about the nature of the hole and electron states and state mixing.

III. RESULTS

Figure 1 shows the energies of the first three lowest hole states in $(\text{GaAs})_n/(\text{AlAs})_n$ superlattices versus the superlattice period n at $\mathbf{k}_{\parallel}=0$. We see that the first three hole states have the order hh1, lh1, and hh2, respectively, and approach the GaAs VBM as the period n increases. On the scale of the figure it is impossible to verify any anticrossing between lh1 and hh2. Thus, Fig. 2 shows a closeup of the region in the box of Fig. 1. The anticrossing gap E_{AC} occurs around the period $n=61$ monolayers and has a value $40 \mu\text{eV}$. The lh1-hh2 coupling potential for $(\text{GaAs})_n/(\text{AlAs})_n$ superlattices is $V_{lh1,hh2} \approx \frac{1}{2}E_{AC} = 20 \mu\text{eV}$. To verify anticrossing behavior we analyze in Fig. 3 the evolution of the wave functions of the two bands with the superlattice period n . At period $n=59$ the second confined hole state is the nodeless lh1 state while the third confined hole state is the two-peak-shaped hh2 state. As n increases from $n=59$, a two-peak structure starts to become evident in the lh1 wave function. At higher periods $n=62$ and $n=63$ the exchange between lh1 and hh2 has already taken place.

Next, we consider $(\text{GaAs})_n/(\text{Ga}_{1-x}\text{Al}_x\text{As})_{\infty}$ quantum wells. As we are interested in the dependence of $V_{lh1,hh2}$ on the barrier height, we vary the band offset value by varying the composition x of the $(\text{Ga}_{1-x}\text{Al}_x\text{As})$ barrier material. We fix the period m of the barrier to a large value $m=74$ corre-

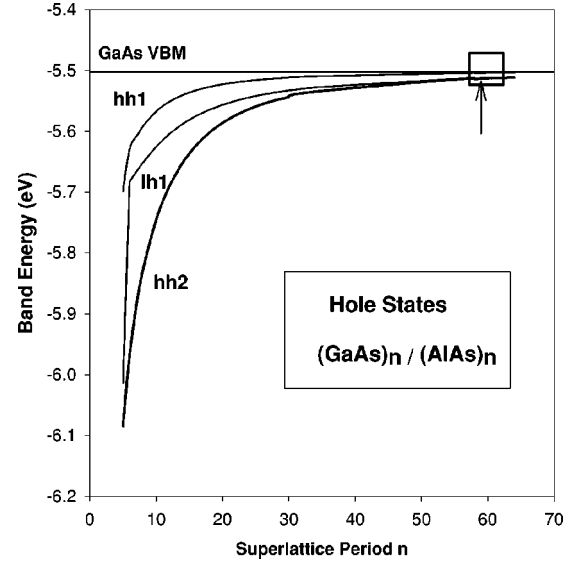


FIG. 1. Energy levels of the three lowest hole states vs the superlattice period n . The position of the GaAs VBM is indicated in figure.

sponding to an impenetrable barrier. We have verified that the results for the first three lowest hole energies obtained with this barrier width are fully reproduced, for all compositions x , when we use a wider barrier with $m=120$ monolayers. The $\text{Ga}_{1-x}\text{Al}_x\text{As}$ alloy is treated through a virtual crystal approximation. The dependence of the barrier height $\Delta E_v(x)$ between the GaAs well and the $\text{Ga}_{1-x}\text{Al}_x\text{As}$ barrier on the Al content x is given in Fig. 4. We see that the barrier height changes between zero and 490 meV with a positive bowing $b=96.8 \text{ meV}$. For each value of the barrier height $\Delta E_v(x)$ (thus alloy composition x) of $(\text{GaAs})_n/(\text{Al}_x\text{Ga}_{1-x}\text{As})_{\infty}$ we have calculated the energies of the lh1 and hh2 states and determined the period n_c at which they anticross. Figure 5 shows n_c versus the barrier height. The resulting trend can be fit by an exponential function (Fig. 5). We see that the anti-

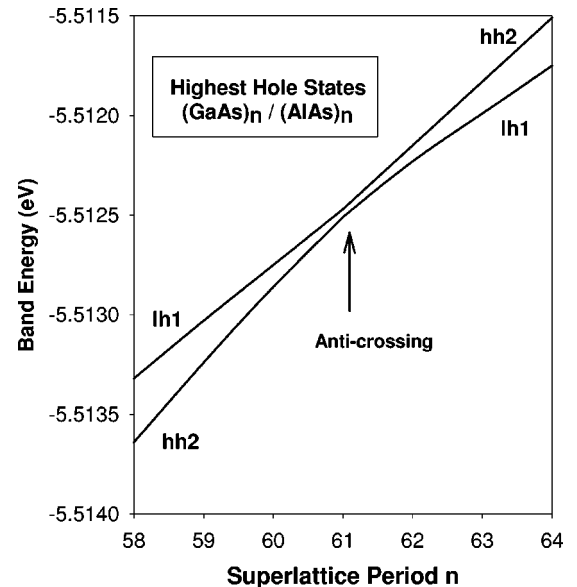


FIG. 2. lh1 and hh2 energy levels in the region of their anticrossing (indicated by an arrow).

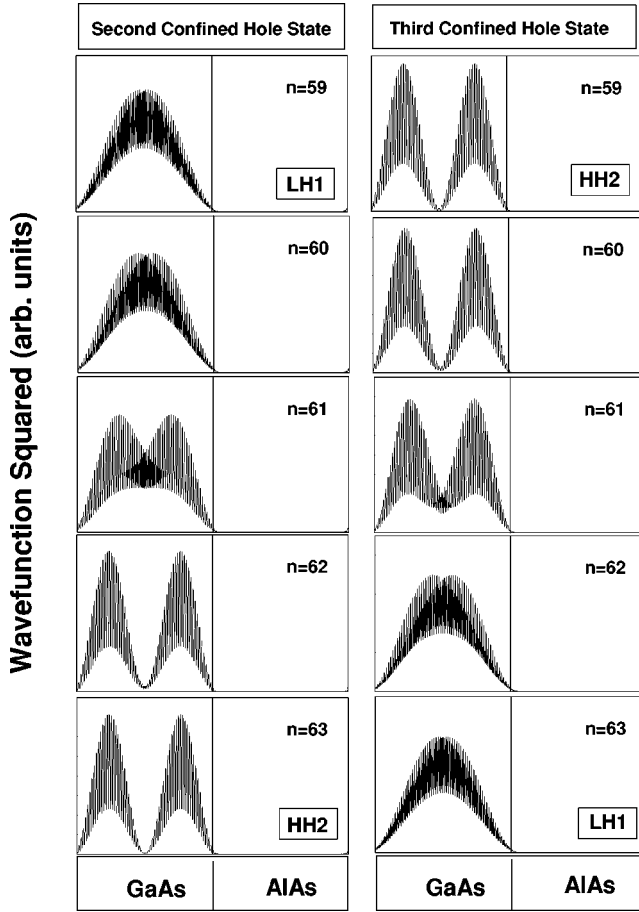


FIG. 3. Evolution of the wave functions of the second confined hole state (left column) and the third confined hole states (right column) of $(\text{GaAs})_n/(\text{AlAs})_n$ superlattices with the superlattice period n . Wave functions are averaged over the in-plane coordinates.

crossing period n_c increases from a lower value $n_c=61$ at $\Delta E_v(x=1)=489$ meV to $n_c=66$ at $\Delta E_v(x=0.1)=40$ meV.

Figure 6 shows the anticrossing gap E_{AC} (approximately twice the $V_{lh1,hh2}$ coupling parameter) versus the barrier height, $\Delta E_v(x)$. We obtain the largest value of E_{AC} at

$\Delta E_v(x=0.2)=82$ meV. The corresponding coupling potential is $V_{lh1,hh2}\approx 0.065$ meV. Note that $V_{lh1,hh2}$ is smaller at higher ΔE_v (higher Al content in the barrier) and is ≈ 0.03 meV at $\Delta E_v=490$ meV ($x=1$). Note also that these values for $V_{lh1,hh2}$ are larger than the value obtained in the case of $(\text{GaAs})_n(\text{AlAs})_n$ superlattices, 0.020 meV (Fig. 2).

To understand the trend of the coupling $V_{lh1,hh2}$ versus barrier height, we refer to an expression derived by Cortez *et al.*²⁷ in the framework of the envelope-function description of the superlattice states:

$$V_{lh1,hh2} = \frac{\Delta E_v}{2\sqrt{3}} f_{lh1}(z_{int}) f_{hh2}(z_{int}) \frac{a}{2}. \quad (4)$$

In this model the coupling potential is taken to be proportional to the product of the envelope-function amplitudes f_{lh1} and f_{hh2} at the interfaces z_{int} times the potential barrier value. To test this model we plot in Fig. 7 ($2V_{lh1,hh2})/(|f_{lh1}(z_{int})| \cdot |f_{hh2}(z_{int})|)$ versus $\Delta E_v(x)$. We use envelope functions f which are directly extracted from our calculated microscopic wave functions, normalized over the unit-cell volume, through a macroscopic average procedure. In this procedure the wave functions are first averaged in the xy planes orthogonal to the growth direction z to obtain $\bar{\psi}(z)$. Then, to eliminate the oscillations along the z direction (which are periodic with a period equal to a monolayer distance), $\bar{\psi}(z)$ are averaged within every monolayer. The resulting envelopes f are then normalized over the superlattice unit cell. We evaluate the envelopes $f(z)$ corresponding to superlattices with periods $n < n_c$, i.e., far from the anticrossing period where the lh1 and hh2 envelopes could be deformed by the coupling and extrapolate at n_c . According to the model of Cortez *et al.* the slope of Fig. 7 should be constant, $a/2\sqrt{3}$. Figure 7 shows that our microscopic calculation does not produce the simple linear scaling implied by Eq. (4). The function plotted increases rapidly at low valence-band offsets whereas at large offset it saturates to a constant value.

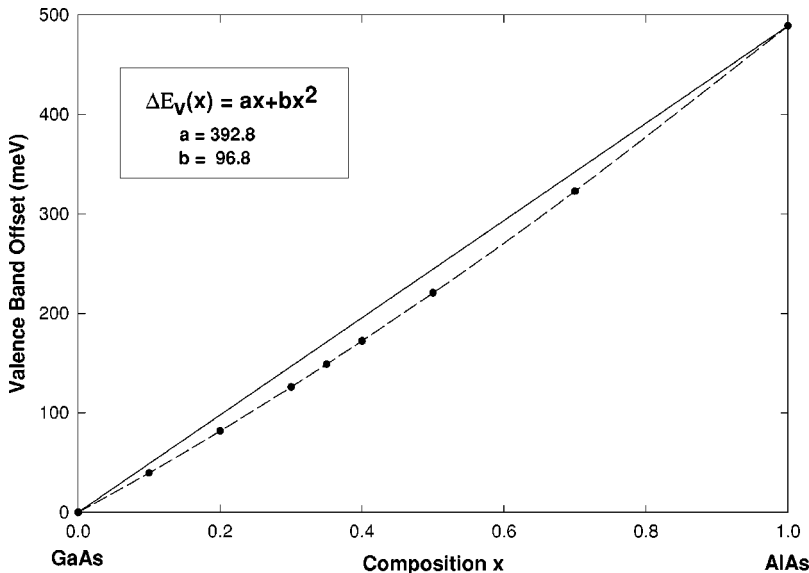


FIG. 4. Valence-band offset between the GaAs valence-band maximum and the $(\text{Al}_x\text{Ga}_{1-x})\text{As}$ valence-band maximum as a function of the composition x of the barrier.

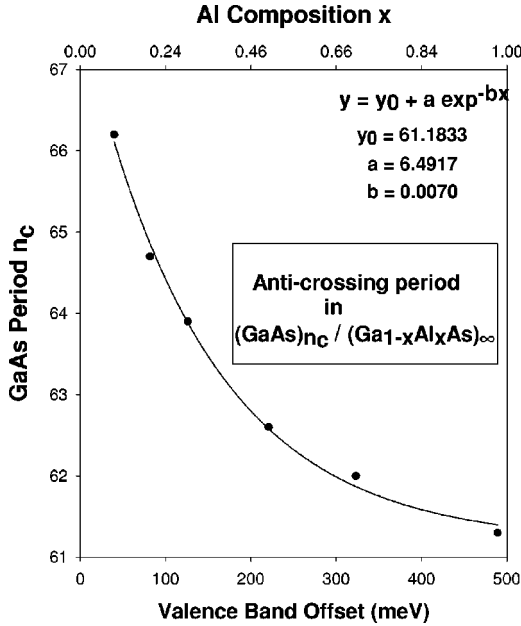


FIG. 5. GaAs quantum well width n_c at which the anticrossing between lh1 and hh2 occurs in $(\text{GaAs})_n/(\text{Al}_x\text{Ga}_{1-x}\text{As})$ quantum wells as a function of the band offset $\Delta E_v(x)$ and the composition x of the barrier.

We can analyze our results for $V_{lh1,hh2}$ versus ΔE_v as follows. For large barrier height the envelope functions are strongly localized *inside* the well, so their amplitude $f(z_{int})$ at the interfaces approaches zero, and $V_{lh1,hh2} \rightarrow 0$. For small barrier height $\Delta E_v \rightarrow 0$ there is no interface anymore, the cubic symmetry is restored, and $V_{lh1,hh2} \rightarrow 0$. Thus, there should be a value of ΔE_v at which the coupling matrix element $V_{lh1,hh2} = |\langle \psi_{lh1} | \Delta V | \psi_{hh2} \rangle|$ between lh1 and hh2 is largest. From Fig. 6 we see that the value of ΔE_v at which the coupling potential is largest is $\Delta E_v \approx 82$ meV (corresponding to $x \approx 0.2$). At higher ΔE_v values the coupling $V_{lh1,hh2}$ diminishes following the trend of the product of the amplitudes $f_{lh1}(z_{int}) \cdot f_{hh2}(z_{int})$ versus ΔE_v given in the inset of Fig. 7. At smaller ΔE_v the smaller potential change ΔV across the interface leads to a smaller coupling.

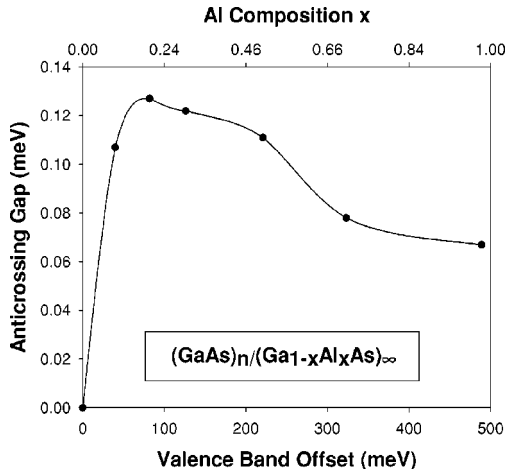


FIG. 6. Anticrossing gap ($\approx 2V_{lh1,hh2}$) vs the band offset between the GaAs well and the $(\text{Al}_x\text{Ga}_{1-x}\text{As})$ barrier in $(\text{GaAs})_n/(\text{Al}_x\text{Ga}_{1-x}\text{As})$ multiple quantum wells.

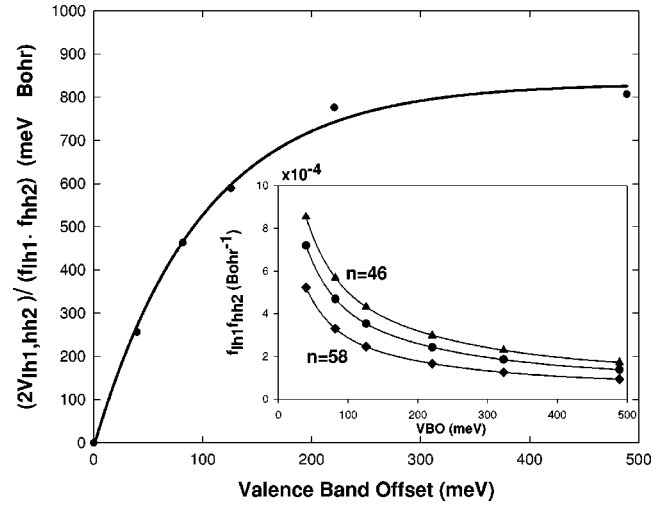


FIG. 7. Trend of the ratio between the coupling $V_{lh1,hh2}$ and the product of the lh1 and hh2 envelopes at the interface vs the band offset value in $(\text{GaAs})_n/(\text{Al}_x\text{Ga}_{1-x}\text{As})$ multiple quantum wells. The best fit of the calculated points is obtained with an exponential function to be compared with the results of the simple model of Eq. (4). The inset shows the product of the envelope functions $f_{lh1}(z_{int}) \cdot f_{hh2}(z_{int})$ vs the band offset for different well widths n .

We see also that for $\Delta E_v < 200$ meV the Cortez *et al.*¹⁷ formula is approximately followed. For $\Delta E_v > 200$ meV we find that $V_{lh1,hh2}$ follows the trend of the product $f_{lh1}(z_{int}) \cdot f_{hh2}(z_{int})$ times a constant, independent of the offset value.

IV. COMPARISON WITH OTHER CALCULATIONS AND EXPERIMENT

We next compare our results for $V_{lh1,hh2}$ with the results of previous calculations. The first (and only) atomistic calculation addressing the anticrossing of lh1 and hh2 at $\mathbf{k}_{\parallel} = 0$ in GaAs/AlAs is the work of Schulman and Chang^{19,35} using an empirical tight-binding approach. To compare our calculated values with those reported by Schulman and Chang³⁵ we need to take into account the different parameters they used to describe the bulk compounds: $\Delta E_v(x=1) = 236$ meV (our value is 489 meV) and for the effective masses of the light-hole and heavy-hole states $m_{hh}^{\text{GaAs}} = 0.45$, $m_{lh}^{\text{GaAs}} = 0.07$, $m_{hh}^{\text{AlAs}} = 0.75$, and $m_{lh}^{\text{AlAs}} = 0.15$, to be compared with our values given in Table II. Their offset value for the GaAs/AlAs heterojunction corresponds to that between GaAs and a $\text{Al}_x\text{Ga}_{1-x}\text{As}$ barrier with $x \approx 0.5$ in our calculation (see Fig. 4). For an infinite barrier with this composition we find anticrossing between lh1 and hh2 at a well width $n_c \approx 63$ monolayers and a gap value 0.11 meV, while Schulman and Chang found anticrossing at much smaller $n_c = 35$ monolayers. No values for the anticrossing gap were reported in their paper.

For a barrier with $m=20$ monolayers of $\text{Al}_{0.3}\text{Ga}_{0.7}\text{As}$ (which has an offset equal to a barrier of composition $x \approx 0.15$ in our calculation) they found anticrossing at a well width $n_c = 70$ monolayers. An anticrossing gap of fractions of meV can be estimated looking at Fig. 6 of Ref. 35. Thus, the order of magnitude of $V_{lh1,hh2}$ extracted from the tight-binding calculation of Schulman and Chang is in substantial

agreement with the values we have obtained with our pseudopotential approach. The different n_c are related to the different bulk parameters.

Ivchenko *et al.*⁶ considered a AlAs/GaAs/AlAs quantum well with a variable number n of GaAs monolayers. They introduced the lh1 and hh2 anticrossing in an *ad hoc* fashion in the envelope-function formalism through the ‘‘generalized boundary conditions,’’ which are equivalent to adding to the Hamiltonian a δ -function term, localized at the interfaces. The coupling potential was expressed in terms of an dimensional parameter t_{lh} multiplied by the product of the lh1 and hh2 envelope-function amplitudes at the interface. They used $m_{hh} = 0.45$, $m_{lh} = 0.09$, $\Delta E_v = 0.53$ eV (similar to our values $m_{hh} = 0.40$, $m_{lh} = 0.11$, $\Delta E_v = 0.49$ eV). Selecting $t_{lh} = 0.5$ they obtained a gap of 1–2 meV at the crossing point $n_c = 50$. This gap is at least *one order of magnitude larger* than the values directly estimated in our atomistic calculations. Also, the trend of the E_{lh1} and E_{hh2} energies versus n , given in Fig. 3(a) of Ref. 6, is such that the minimum difference between them (the anticrossing gap E_{AC}), is not achieved at $n = n_c$ [the value of n at which lh1 and hh2 exchange their character, see also Fig. 3(c) of Ref. 6] as it is in the atomistic calculations. Obviously, the interaction potential parameter $t_{lh} = 0.5$ is too strong. Our atomistic calculations show that $V_{lh1,hh2}$ is smaller, of the order of tens or hundreds of meV, and its effect on the hole energies is seen essentially only at $n \approx n_c$. At smaller or larger n , $E_{lh1} = E_{lh1}^0$ and $E_{hh2} = E_{hh2}^0$, where E_{lh1}^0 and E_{hh2}^0 indicate the uncoupled lh1 and hh2 energies. The differences between the model Hamiltonian approach⁶ and our atomistic approach highlight the fact that the former approach depends on parameters it cannot calculate.

On the experimental side, the effect of the lh1 and hh2 coupling in D_{2d} systems is seen in the appearance of dipole-forbidden $e1$ -hh2 and $e2$ -lh1 exciton features.^{17,18} From the excitation spectra of $(\text{GaAs})_{36}/(\text{Al}_{0.27}\text{Ga}_{0.73}\text{As})_{74}$ multiple quantum wells, the energy difference between the dipole-allowed $e_{1l} = (\text{lh1}-e1)$ and the dipole-forbidden $e_{12h} = (\text{hh2}-e1)$ excitons and between the dipole-forbidden $e_{21l} = (\text{lh1}-e2)$ and the dipole-allowed $e_{2h} = (\text{hh2}-e2)$ excitons can be estimated in both cases to be about 10 meV. In our single-particle calculation when the splitting between E_{lh1} and E_{hh2} is 10 meV, the light-hole and heavy-hole states are only weakly coupled. However, a calculation of a full excitonic spectrum, which is beyond our single-particle approach, would be necessary to assess the intensities of these transitions and afford a direct comparison with this experiment.

V. DIPOLE TRANSITION STRENGTHS

Figure 8 shows the dipole matrix elements for transitions from the second valence subband (denoted as V2) and the third valence subband (denoted as V3) to the two lowest conduction subbands, $e1$ and $e2$, for a $(\text{GaAs})_n/(\text{Al}_{0.2}\text{Ga}_{0.8}\text{As})_{m=74}$ quantum well, as a function of the number n of GaAs layers in the well. We see that the dipole transition probabilities show a mirrorlike behavior across the value $n_c = 64.7$ which corresponds to the calculated period n_c of the anticrossing between lh1 and hh2. For $n < n_c$ the calculated transition probabilities indicate that the

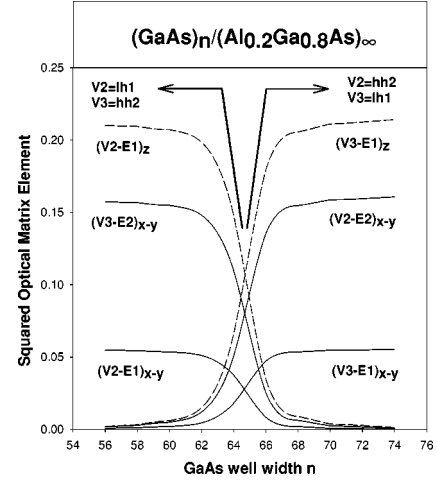


FIG. 8. Squared optical matrix elements of the interband transitions from the lh1-hh2 coupled hole states denoted as V1 and V2 to the first two electron states $e1$ and $e2$ for $(\text{GaAs})_n/(\text{Al}_{0.2}\text{Ga}_{0.8}\text{As})$ multiple quantum wells. The squared optical matrix elements are plotted as a function of the number n of GaAs layers.

subband $V2 = \text{lh1}$ and $V3 = \text{hh2}$, while for $n > n_c$ the roles of $V2$ and $V3$ are exchanged. This calculation provides another way to study the mixing transition between $lh1$ and $hh2$ and determine the anticrossing point n_c . We see from this result that the transition takes place over just three monolayers. The calculations of Chang and Schulman¹⁹ showed a much more gradual transition with the well width n .

From Fig. 8 we also see that there is a dependence of the transition probability on the polarization direction along z or in the x - y plane. The transitions to the $e2$ electron state are completely in-plane polarized while those to the $e1$ state are *mainly* polarized along z . No in-plane polarization anisotropy between the $[110]$ and $[-110]$ directions is observed for any transitions. This can be understood by observing that the overall symmetry of these systems is the D_{2d} point group which leads to an off-diagonal dielectric tensor element $\epsilon_{xy} = 0$ (Ref. 14) and, consequently, to a zero in-plane polarization anisotropy (see the caption to Table I). Thus, we find a zero in-plane polarization anisotropy related to the mixing of lh1 and hh2 hole states. This result is in agreement with the experimental data which have not observed in-plane anisotropy in the optical absorption of common atom superlattices.

VI. SUMMARY

We conducted an atomistic calculation of the coupling potential $V_{lh1,hh2}$ between the lh1 and hh2 hole states in common atom (001) GaAs/AlAs superlattices and quantum wells of symmetry D_{2d} . The D_{2d} symmetry of these systems is caused by the compensation of the effects of the single (001) interfaces (whose symmetry is C_{2v}), which takes place when the two interfaces are equal. We address here, in particular, the issue of the strength of the lh1 and hh2 coupling, $V_{lh1,hh2}$, at $\mathbf{k} \parallel 0$. This coupling has been previously invoked to explain quantitatively the experimentally observed forbidden transitions in excitation spectra,¹⁸ but its value cannot be provided by the ‘‘standard’’ $\mathbf{k} \cdot \mathbf{p}$ approach, which neglects this coupling. Atomistic calculations, which naturally include the proper symmetries can directly provide the neces-

sary values for the coupling strength. We have calculated the strength of $V_{lh1,hh2}^{k_{\parallel}=0}$ through the evaluation of the anticrossing gap which opens between the lh1 and hh2 energies when they get closer to each other. This evaluation has been performed for $(\text{GaAs})_n/(\text{AlAs})_n$ superlattices and for $(\text{GaAs})_n/(\text{Al}_x\text{Ga}_{1-x}\text{As})_{m=\infty}$ quantum wells, where the Al content of the barrier x has been varied from 0.1 to 1.0. At a critical period $n=n_c$, anticrossing between the lh1 and hh2 states is calculated. Our calculations show that the strength of $V_{lh1,hh2}$ is very small, of the order of magnitude 0.05 meV, in all the systems we have studied. The smallness of this interaction causes the lh1 and hh2 states to mix and form an anticrossing gap only for periods that are within a few monolayers of the critical size n_c at which anticrossing occurs. This happens at a period $n_c \approx 61$ in $(\text{GaAs})_n/(\text{AlAs})_n$ superlattices with a gap about 0.040 meV wide. Also in $(\text{GaAs})_n/(\text{Al}_x\text{Ga}_{1-x}\text{As})_{m=\infty}$ multiple quantum wells the anticrossing well width n_c varies between 61 and 67 as a function of the Al barrier composition x . The anticrossing gap E_{AC} (and $V_{lh1,hh2}$) depends on the composition x of the barrier and, since the valence-band offset ΔE_v between the well

and the barrier depends on the barrier composition, the anticrossing gap depends on ΔE_v . We have found that for GaAs quantum wells embedded in $\text{Al}_x\text{Ga}_{1-x}\text{As}$ barriers, the coupling between the lh1 and hh2 states, $V_{lh1,hh2}$, is maximum when the composition of the barrier is $x \approx 0.2$, which corresponds to a offset in a range from 80 to 100 meV. Our results allow us to test some recently proposed models^{6,27} for hole coupling. We have found that for $\Delta E_v < 200$ meV, $V_{lh1,hh2}/(f_{lh1} \cdot f_{hh2})$ (f is the envelope function amplitude at the interface) increases with the offset value while in the range $\Delta E_v > 200$ meV the strength of $V_{lh1,hh2}/(f_{lh1} \cdot f_{hh2})$ remains constant with ΔE_v .

ACKNOWLEDGMENTS

Work at the Dipartimento di Fisica di Modena was supported by the Italian MURST Project No. COFIN99 and by No. INTAS-99-15 and work at NREL was supported by DOE-SC-BES-DMS under Contract No. DE-AC36-98-GO10337. We acknowledge useful discussions with P. Voisin, O. Krebs, and S. Cortez.

- ¹A. Zunger, S.-H. Wei, L.G. Ferreira, and J.E. Bernard, Phys. Rev. Lett. **65**, 353 (1990); R. Magri, S. Froyen, and A. Zunger, Phys. Rev. B **44**, 7947 (1991).
- ²J.E. Bernard, S.H. Wei, D.M. Wood, and A. Zunger, Appl. Phys. Lett. **52**, 311 (1987).
- ³W. Shan, W. Walukiewicz, J.W. Ager III, E.E. Haller, J.F. Geisz, D.J. Friedman, J.M. Olson, and S.R. Kurtz, Phys. Rev. Lett. **82**, 1221 (1999).
- ⁴S.H. Wei, and A. Zunger, Phys. Rev. B **37**, 8958 (1988).
- ⁵J.E. Jaffe and A. Zunger, Phys. Rev. B **29**, 1882 (1984).
- ⁶E.L. Ivchenko, A.Yu. Kaminski, and U. Rossler, Phys. Rev. B **54**, 5852 (1996).
- ⁷O. Krebs and P. Voisin, Phys. Rev. Lett. **77**, 1829 (1996); O. Krebs, D. Rondi, J.L. Gentner, L. Goldstein, and P. Voisin, *ibid.* **80**, 5770 (1998).
- ⁸S.H. Kwok, H.T. Grahn, K. Ploog, and R. Merlin, Phys. Rev. Lett. **69**, 973 (1993).
- ⁹Y.H. Chen, Z. Yang, Z.G. Wang, X. Bo, and J.B. Liang, Phys. Rev. B **60**, 1783 (1999).
- ¹⁰B. Koopmans, P.V. Santos, and M. Cardona, Phys. Status Solidi A **170**, 307 (1998).
- ¹¹C. Gourdon and P. Lavallard, Phys. Rev. B **46**, 4644 (1992).
- ¹²G.E. Pikus and F.G. Pikus, Solid State Commun. **89**, 319 (1994).
- ¹³G. Edwards and J.C. Inkson, Solid State Commun. **89**, 595 (1994).
- ¹⁴R. Magri and S. Ossicini, Phys. Rev. B **58**, R1742 (1998).
- ¹⁵L.W. Wang, S.H. Wei, T. Mattila, A. Zunger, I. Vurgaftman, and J.R. Meyer, Phys. Rev. B **60**, 5590 (1999).
- ¹⁶R. Magri, L.W. Wang, A. Zunger, I. Vurgaftman, and J.R. Meyer, Phys. Rev. B **61**, 10 235 (2000).
- ¹⁷R.C. Miller, A.C. Gossard, G.D. Sanders, Y.-C. Chang, J.N. Schulman, Phys. Rev. B **32**, R8452 (1985).
- ¹⁸W.M. Theis, G.D. Sanders, C.E. Leak, D.C. Reynolds, Y.-C. Chang, K. Alavi, C. Colvard, and I. Shidlovsky, Phys. Rev. B **39**, R1442 (1989); D.C. Reynolds, K.K. Bajaj, C.E. Leak, G. Peters, W. Theis, P.W. Yu, K. Alavi, C. Colvard, and I. Shidlovsky, *ibid.* **37**, R3117 (1988).
- ¹⁹Y.-C. Chang and J.N. Schulman, Appl. Phys. Lett. **43**, 536 (1983).
- ²⁰G. Bastard, *Wave Mechanics Applied to Semiconductor Heterostructures* (Les Editions de Physique, Paris, 1988).
- ²¹O. Krebs, W. Seidel, J.P. André, D. Bertho, C. Jouanin, and P. Voisin, Solid State Commun. **12**, 938 (1997).
- ²² Γ -X coupling is zero in the tight-binding calculation of J.G. Menchero *et al.*, Phys. Rev. Lett. **10**, 2034 (1999), unless one adds “by hand” a term.
- ²³M.G. Burt, Phys. Rev. B **50**, 7518 (1994); Appl. Phys. Lett. **65**, 717 (1994); J. Phys.: Condens. Matter **4**, 6651 (1992).
- ²⁴B.A. Foreman, Phys. Rev. Lett. **81**, 425 (1998).
- ²⁵D.L. Smith and C. Mailhot, Rev. Mod. Phys. **62**, 173 (1990).
- ²⁶J.B. Xia, Phys. Rev. B **41**, 3117 (1990).
- ²⁷S. Cortez, O. Krebs, and P. Voisin, J. Vac. Sci. Technol. B **18**, 2232 (2000).
- ²⁸K.A. Mader and A. Zunger, Phys. Rev. B **50**, 17 393 (1994).
- ²⁹D.M. Wood and A. Zunger, Phys. Rev. B **53**, 7949 (1996).
- ³⁰W. Ge, W.D. Schmidt, M.D. Sturge, L.N. Pfeiffer, and K.W. West, J. Lumin. **59**, 163 (1994).
- ³¹G. Li, D. Jiang, H. Han, Z. Wang, and K. Ploog, Phys. Rev. B **40**, 10 430 (1989).
- ³²S.B. Zhang, M.L. Cohen, S.G. Louie, D. Tomanek, and M.S. Hybertsen, Phys. Rev. B **41**, 10 058 (1990).
- ³³L.W. Wang and A. Zunger, Phys. Rev. B **51**, 17 398 (1995).
- ³⁴L.W. Wang and A. Zunger, J. Chem. Phys. **100**, 2394 (1994).
- ³⁵J.N. Schulman and Y.C. Chang, Phys. Rev. B **31**, 2056 (1985).